GEOPHYSICS, VOL. 65, NO. 6 (NOVEMBER-DECEMBER 2000); P. 1788–1802, 8 FIGS.

Estimation of fracture parameters from reflection seismic data—Part I: HTI model due to a single fracture set

Andrey Bakulin*, Vladimir Grechka‡, and Ilya Tsvankin‡

ABSTRACT

The simplest effective model of a formation containing a single fracture system is transversely isotropic with a horizontal symmetry axis (HTI). Reflection seismic signatures in HTI media, such as NMO velocity and amplitude variation with offset (AVO) gradient, can be conveniently described by the Thomsen-type anisotropic parameters $\epsilon^{(V)}$, $\delta^{(V)}$, and $\gamma^{(V)}$. Here, we use the linear slip theory of Schoenberg and co-workers and the models developed by Hudson and Thomsen for penny-shaped cracks to relate the anisotropic parameters to the physical properties of the fracture network and to devise fracture characterization procedures based on surface seismic measurements.

Concise expressions for $\epsilon^{(V)}$, $\delta^{(V)}$, and $\gamma^{(V)}$, linearized in the crack density, show a substantial difference between the values of the anisotropic parameters for isolated fluid-filled and dry (gas-filled) penny-shaped cracks. While the dry-crack model is close to elliptical with $\epsilon^{(V)} \approx \delta^{(V)}$, for thin fluid-filled cracks $\epsilon^{(V)} \approx 0$ and the absolute value of $\delta^{(V)}$ for typical V_S/V_P ratios in the background is close to the crack density. The parameters $\epsilon^{(V)}$ and $\delta^{(V)}$ for models with partial saturation or hydraulically connected cracks and pores always lie between the values for dry and isolated fluid-filled cracks. We also demonstrate that all possible pairs of $\epsilon^{(V)}$ and $\delta^{(V)}$ occupy a relatively narrow triangular area in the $[\epsilon^{(V)}, \delta^{(V)}]$-plane, which can be used to identify the fracture-induced HTI model from seismic data.

The parameter $\delta^{(V)}$, along with the fracture orientation, can be obtained from the P-wave NMO ellipse for a horizontal reflector. Given $\delta^{(V)}$, the NMO velocity of a dipping event or nonhyperbolic moveout can be inverted for $\epsilon^{(V)}$. The remaining anisotropic coefficient, $\gamma^{(V)}$, can be determined from the constraint on the parameters of vertically fractured HTI media if an estimate of the V_S/V_P ratio is available. Alternatively, it is possible to find $\gamma^{(V)}$ by combining the NMO ellipse for horizontal events with the azimuthal variation of the P-wave AVO gradient. Also, we present a concise approximation for the AVO gradient of converted (PS) modes and show that all three relevant anisotropic coefficients of HTI media can be determined by the joint inversion of the AVO gradients or NMO velocities of P- and PS-waves.

For purposes of evaluating the properties of the fractures, it is convenient to recalculate the anisotropic coefficients into the normal (Δ_N) and tangential (Δ_T) weaknesses of the fracture system. If the HTI model results from penny-shaped cracks, Δ_T gives a direct estimate of the crack density and the ratio Δ_N/Δ_T is a sensitive indicator of fluid saturation. However, while there is a substantial difference between the values of Δ_N/Δ_T for isolated fluid-filled cracks and dry cracks, interpretation of intermediate values of Δ_N/Δ_T for porous rocks requires accounting for the hydraulic interaction between cracks and pores.

INTRODUCTION

Seismic detection of subsurface fractures has important applications in characterization of naturally fractured reservoirs. It is well known that preferential orientation of fracture networks makes the medium azimuthally anisotropic with respect to seismic wave propagation. Although the presence of azimuthal anisotropy has a strong influence on all propagation modes (i.e., P-, S-, and converted waves), most existing studies concentrate on analysis of time delays or reflection amplitudes of split shear waves at near-vertical incidence.

Manuscript received by the Editor April 16, 1999; revised manuscript received February 28, 2000.
*Formerly St. Petersburg State University, Department of Geophysics, St. Petersburg, Russia. Presently Schlumberger Cambridge Research, High Cross, Madingley Road, Cambridge CB 3 0EL, England. E-mail: bakulin@cambridge.scr.slb.com.
‡Colorado School of Mines, Center for Wave Phenomena, Department of Geophysics, Golden, Colorado 80401-1887. E-mail: vgrechka@dix.mines.edu; ilya@dix.mines.edu.

While such measurements make it possible to map the orientation and intensity (or crack density) of a vertical fracture set, they are not sensitive to the fracture infill (content), unless the fractures are corrugated (see part III of this series). Recently, it was demonstrated that the azimuthal dependence of P-wave signatures has the potential of not only constraining the fracture orientation (e.g., Corrigan et al., 1996) and density (Tsvankin, 1997) but also of discriminating between dry (gas-filled) and fluid-filled fractures (Sayers and Rickett, 1997; Rüger and Tsvankin, 1997). Further progress in seismic methods of fracture detection, however, requires a better understanding of the relationship between the anisotropic parameters measured from seismic data and the physical properties of fracture systems.

This is the first of three papers in which we discuss anisotropic seismic signatures associated with vertical fracture sets. The transversely isotropic medium with a horizontal axis of symmetry (HTI), addressed here, is the simplest anisotropic model caused by parallel rotationally invariant vertical fractures in isotropic host (background) rock. In the two sequel papers we study more complicated orthorhombic and monoclinic models needed to describe multiple fracture sets and/or formations with an anisotropic background. Among the main questions we will attempt to answer are these:

1) Do different theories of seismic wave propagation in fractured media (e.g., those by Hudson, 1980, 1981; Schoenberg, 1980, 1983; Thomsen, 1995; Hudson et al., 1996) lead to the same effective anisotropic model?
2) What is the relationship between the anisotropic parameters that control seismic signatures and the physical properties of the fractures?
3) What types of seismic data are needed to obtain information about various properties of fracture systems?
4) What characteristics of fractured formations (e.g., crack density, fracture azimuth, equant porosity, type of infill) can be evaluated using surface reflection data?

While our ultimate goal is to invert seismic data for the physical characteristics of fracture networks, the data are controlled by the elastic parameters (e.g., by the stiffness tensor) of the effective anisotropic medium. The effective parameters depend not only on the orientation, compliances, etc., of the fractures but also on the elastic properties of the (possibly anisotropic) host rock. Taken together, the characteristics of the fractures and host rock form a set of so-called microstructural parameters. Even though seismic data may provide sufficient information to recover the effective anisotropic model, it may be impossible to obtain the microstructural parameters individually. Indeed, with increasing complexity of the fractured model (e.g., in the presence of multiple dipping fracture sets), the number of microstructural parameters can become arbitrarily large, whereas the maximum number of the effective anisotropic parameters is just 21 for the most general media of triclinic symmetry. Still, we will show that, for a range of fracture models, seismic data can be inverted for some particular microstructural parameters responsible for practically important properties of the fractured medium.

To identify the fracture parameters constrained by seismic data, it is useful to compare the results of different approaches to effective medium theory. Effective models of fractured media discussed below include those based on parallel infinite fractures with linear slip boundary conditions (Schoenberg, 1980, 1983), isolated parallel penny-shaped cracks that have the form of oblate spheroids (Hudson, 1980, 1981), and partially saturated penny-shaped cracks or hydraulically connected cracks and pores (Hudson, 1988; Thomsen, 1995; Hudson et al., 1996). An important result in establishing the relationships between different theories is obtained by Schoenberg and Douma (1988), who prove that infinite parallel fractures with linear slip (Schoenberg, 1980, 1983) and penny-shaped cracks (Hudson, 1980, 1981) yield the same structure of the effective stiffness tensor (i.e., it is impossible to distinguish between the two models just by inspecting the stiffnesses). This is a clear indication that seismic data are not sensitive to one of the microstructural parameters: the shape of the fractures. Further generalizing this result, we demonstrate that the presence of equant porosity with hydraulic connection to the cracks and/or partial saturation does not change the structure of the stiffness tensor. The values of the anisotropic coefficients in this case turn out to be intermediate between those for isolated fluid-filled and dry cracks.

Reflection seismic signatures in anisotropic media are most concisely described by Thomsen-type dimensionless anisotropic coefficients, such as the parameters ϵ, δ, and γ originally introduced by Thomsen (1986) for transverse isotropy with a vertical symmetry axis (VTI media). These coefficients capture the influence of anisotropy on various seismic signatures and therefore can be determined from seismic data. Most existing work on effective parameters of fractured media (e.g., Hudson, 1981; Schoenberg, 1983), however, is formulated in terms of the stiffnesses c_{ij} or compliances s_{ij}. Better understanding of the influence of cracks on reflection seismic signatures requires expressing these results through Thomsen-type anisotropic coefficients. For the VTI medium due to a single system of horizontal fractures, Schoenberg and Douma (1988) obtain the weak-anisotropy approximations for Thomsen's (1986) anisotropic parameters and note that only two out of the three coefficients (ϵ, δ, γ) are independent. Thomsen (1995) presents more general expressions for ϵ, δ, and γ of a similar VTI model that contains horizontal fractures hydraulically connected to pore space.

For HTI media resulting from vertical, rotationally invariant fractures, reflection traveltimes and amplitudes are convenient to express through the Thomsen-type parameters $\epsilon^{(V)}$, $\delta^{(V)}$, and $\gamma^{(V)}$ described by Rüger (1997) and Tsvankin (1997). [Note that $\epsilon^{(V)}$, $\delta^{(V)}$, and $\gamma^{(V)}$ are different from the generic Thomsen parameters defined with respect to the horizontal symmetry axis.] Approximate expressions for $\epsilon^{(V)}$ and $\delta^{(V)}$ are derived by Sayers and Rickett (1997), who use them to study the azimuthal variation of the P-wave amplitude variation with offset (AVO) response. Here, we give a systematic analysis of the dependence of the anisotropic coefficients of HTI media on the physical properties of vertical fractures.

After a brief discussion of geological data on fractures, we review the linear slip theory following the work of Schoenberg (1983), Schoenberg and Douma (1988), and Schoenberg and Sayers (1995). This theory, based on physically intuitive relations between stress and discontinuity in displacement, is formulated in terms of the fracture compliances or weaknesses and requires no assumptions about the microstructure and microgeometry of fractures. Then we obtain the anisotropic coefficients of the effective HTI solid as functions of the

fracture weaknesses and determine the bounds of $\epsilon^{(V)}$ and $\delta^{(V)}$ for arbitrary strength of fracturing. For models with penny-shaped (spheroidal) cracks, the anisotropic coefficients and weaknesses are expressed through the microstructural parameters using the theories of Hudson (Hudson , 1981, 1988; Hudson et al., 1996) and Thomsen (1995). Extending the results of Tsvankin (1997) and Contreras et al. (1999), we show that a complete fracture characterization procedure (including evaluation of the fluid content) can be based on (1) conventional P-wave data recorded in wide-azimuth 3-D surveys or (2) the combination of P-waves and converted PS-waves.

EFFECTIVE MODELS OF FRACTURED MEDIA

Geological background

A concise overview of the properties of natural fracture systems can be found, for example, in Aguilera (1998). Subsurface fractures usually occur in large populations or sets with similar orientations. Fracture openings (apertures) may vary from very thin (0.001–0.01 mm) to relatively wide (0.1–0.5 mm), but it is believed that in-situ values do not deviate substantially from an average of 0.02 to 0.03 mm (Romm, 1985). Aguilera (1998), however, mentions that in some reservoirs where fractures are propped by partial mineralization, the apertures may reach 1 inch or more.

An important parameter of a fracture set is the distance between the adjacent fractures, which is much greater than the fracture opening. Conventionally, geologists describe fractured rocks by the so-called fracture intensity,

$$\text{fracture intensity} = \frac{\text{number of fractures}}{\text{meter}},$$

with the number of fractures counted in the direction perpendicular to the fracture planes. Fracture intensity for very sparse sets is less than 0.75 m^{-1}, while for tight sets it may exceed 10 m^{-1} (Bagrintseva, 1982). Typical values of fracture intensity for carbonate reservoirs are estimated as 1–20 m^{-1} (Kirkinskaya and Smekhov, 1981).

Since seismic wavelengths are on the order of tens and hundreds of meters, it is clear that

$$\text{seismic wavelength} \gg \text{fracture spacing} \gg \text{fracture opening}.$$

Therefore, in building effective seismological models we can neglect finite fracture openings and details of the spatial distributions of fractures and can consider fractured blocks as equivalent or effective anisotropic solids (i.e., use the long-wavelength approximation). The parameters of such an effective model will depend on the orientation and intensity of the fracture set(s) and the properties of the material filling the fractures, as well as on the elastic coefficients of the host rock.

Parallel fractures: The linear slip model

To obtain the effective parameters of fractured media, Schoenberg (1980, 1983) suggests treating the fractures, regardless of their shape and microstructure, as either infinitely thin and highly compliant (soft) layers or planes of weakness with linear-slip (nonwelded, see below) boundary conditions. While these two representations are equivalent in the long-wavelength limit, each is useful in developing effective models of fractured rock and gaining insight into the physical meaning of the fracture parameters.

The most straightforward way to derive the parameters of the effective medium is to apply the approach based on the thin-layer model. The exact Backus (1962) averaging procedure for parallel thin, soft layers embedded in an isotropic matrix leads to the following simple form of the effective compliance matrix $\mathbf{s}$ (the inverse of the stiffness matrix $\mathbf{c}$):

$$\mathbf{s} = \mathbf{s}_b + \mathbf{s}_f, \tag{1}$$

where $\mathbf{s}_b$ is the compliance matrix of the host rock and $\mathbf{s}_f$ is the excess compliance associated with the layers (Schoenberg and Muir, 1989; Molotkov and Bakulin, 1997). Although it would be more natural to denote stiffness by s and compliance by c, the notation used here is widely cited in the literature on elasticity and wave propagation.

It may be proved by means of the reflectivity (matrix) method that for vertical layers orthogonal to the x_1-axis, $\mathbf{s}_f$ is given by

$$\mathbf{s}_f = \nu \begin{pmatrix} s_{11\,f} & 0 & 0 & 0 & s_{15\,f} & s_{16\,f} \\ 0 & 0 & 0 & 0 & 0 & 0 \\ 0 & 0 & 0 & 0 & 0 & 0 \\ 0 & 0 & 0 & 0 & 0 & 0 \\ s_{15\,f} & 0 & 0 & 0 & s_{55\,f} & s_{56\,f} \\ s_{16\,f} & 0 & 0 & 0 & s_{56\,f} & s_{66\,f} \end{pmatrix}. \tag{2}$$

Here, ν is the fraction of the total volume occupied by the thin layers and $s_{ij\,f}$ are the compliances of the layers' material. As follows from equations (1) and (2), only six compliance elements contribute to the effective parameters. Although ν is assumed to be small, all compliances $s_{ij\,f}$ are large (i.e., the material is soft) and the products $\nu s_{ij\,f}$ are finite. The general condition of the medium's stability also requires that the 3×3 submatrix composed of the nonzero elements of the compliance matrix (2) be nonnegative definite.

Equation (2) can also be used to describe a set of parallel fractures of infinite extent with the fracture normal $\mathbf{n}$ parallel to the x_1-axis. Following Schoenberg (1980), we treat fractures as planes of weakness with nonwelded boundary conditions. For the purpose of deriving the effective parameters, the medium containing parallel planes of weakness is equivalent to the thin-layer model discussed above. Therefore, the matrix of the excess fracture compliances can be written as

$$\mathbf{s}_f = \begin{pmatrix} K_N & 0 & 0 & 0 & K_{NV} & K_{NH} \\ 0 & 0 & 0 & 0 & 0 & 0 \\ 0 & 0 & 0 & 0 & 0 & 0 \\ 0 & 0 & 0 & 0 & 0 & 0 \\ K_{NV} & 0 & 0 & 0 & K_V & K_{VH} \\ K_{NH} & 0 & 0 & 0 & K_{VH} & K_H \end{pmatrix}. \tag{3}$$

The jumps in the stress tensor (σ_{ij}) and displacement vector ($\mathbf{u}$) across a plane of weakness satisfy the boundary conditions of linear slip (Schoenberg, 1980; Molotkov and Bakulin, 1997):

$$[\sigma_{11}] = [\sigma_{12}] = [\sigma_{13}] = 0,$$
$$[u_1] = h(K_N\sigma_{11} + K_{NH}\sigma_{12} + K_{NV}\sigma_{13}),$$
$$[u_2] = h(K_{NH}\sigma_{11} + K_H\sigma_{12} + K_{VH}\sigma_{13}),$$
$$[u_3] = h(K_{NV}\sigma_{11} + K_{VH}\sigma_{12} + K_V\sigma_{13}), \qquad (4)$$

where h is the average distance (spacing) between the fractures and the brackets denote the jump of the corresponding value across the interface (plane of weakness).

Equations (4) help explain the physical meaning of the compliances K_N, K_V, K_H, K_{NV}, K_{NH}, and K_{VH}. For instance, K_N is the normal fracture compliance relating the jump of the normal (to the fractures) displacement u_1 to the normal stress σ_{11}. Likewise, K_V and K_H are the two shear compliances along the vertical (x_3) and horizontal (x_2) directions. The compliance K_{NV} is the coupling factor between the jump of the normal displacement u_1 and the shear stress σ_{13} or, equivalently, between u_3 and σ_{11}. Such a coupling may be caused by a slight roughness (corrugation) of the fracture surfaces, with peaks and troughs somewhat offset from one side of the fracture to the other (Schoenberg and Douma, 1988).

From the physical point of view, a nonzero K_{NV} implies that the normal and shear slips with respect to the fracture plane (u_1 and u_3) are coupled. Since a nonzero element K_{NV} in matrix (3) yields a nonzero compliance $s_{15\,f}$ in equation (2), a fracture set with $K_{NV} \neq 0$, $K_{NH} = K_{VH} = 0$ produces a medium of monoclinic symmetry, and is sometimes called monoclinic (Schoenberg and Douma, 1988). The same type of coupling is associated with nonzero values of K_{NH} and K_{VH}. However, as shown by Berg et al. (1991), K_{VH} (unlike K_{NV} and K_{NH}) can always be eliminated by a proper rotation of the coordinate frame around the direction normal to the fractures.

Using largely physical (rather than rigorous mathematical) arguments, the above results are generalized by Nichols et al. (1989) for multiple sets of fractures of infinite extent and by Schoenberg and Sayers (1995) for thin fractures of arbitrary shape and finite dimensions. In particular, the linear addition of the fracture compliances to the compliance of the host rock [equation (1)] is applied by these authors to noninteracting multiple fracture sets.

Hereafter, we consider the simplest form of the matrix of the excess fracture compliance by assuming no coupling between the slips along the coordinate directions and a purely isotropic microstructure of the fracture surfaces. For fracture sets with these properties [called rotationally invariant by Schoenberg and Sayers (1995)], the elements of the compliance matrix satisfy the following relationships (Hsu and Schoenberg, 1993):

$$K_{NV} = K_{NH} = K_{VH} = 0, \quad K_V = K_H \qquad (5)$$

As a result, the matrix of fracture compliances (3) reduces to

$$\mathbf{s}_f = \begin{pmatrix} K_N & 0 & 0 & 0 & 0 & 0 \\ 0 & 0 & 0 & 0 & 0 & 0 \\ 0 & 0 & 0 & 0 & 0 & 0 \\ 0 & 0 & 0 & 0 & 0 & 0 \\ 0 & 0 & 0 & 0 & K_T & 0 \\ 0 & 0 & 0 & 0 & 0 & K_T \end{pmatrix}, \qquad (6)$$

where $K_V = K_H$ is denoted by K_T. The values K_N and K_T are nonnegative and have the physical meaning of the normal and tangential compliances added by the fractures to the host rock. For a purely isotropic background model characterized by the Lamé constants λ and μ, Hsu and Schoenberg (1993) introduce dimensionless quantities

$$\Delta_N = \frac{(\lambda + 2\mu)K_N}{1 + (\lambda + 2\mu)K_N}, \qquad (7)$$

$$\Delta_T = \frac{\mu K_T}{1 + \mu K_T}. \qquad (8)$$

From this definition it is clear that both Δ_N and Δ_T, which we call the normal and tangential *weaknesses* (Bakulin and Molotkov, 1998), vary from 0 to 1.

Using equations (1) and (6) and inverting the compliance matrix yields the stiffness matrix of the effective fractured medium (Schoenberg and Sayers, 1995):

$$\mathbf{c} = \mathbf{s}^{-1} = \mathbf{c}_b - \begin{pmatrix} (\lambda + 2\mu)\Delta_N & \lambda\Delta_N & \lambda\Delta_N & 0 & 0 & 0 \\ \lambda\Delta_N & \dfrac{\lambda^2}{\lambda + 2\mu}\Delta_N & \dfrac{\lambda^2}{\lambda + 2\mu}\Delta_N & 0 & 0 & 0 \\ \lambda\Delta_N & \dfrac{\lambda^2}{\lambda + 2\mu}\Delta_N & \dfrac{\lambda^2}{\lambda + 2\mu}\Delta_N & 0 & 0 & 0 \\ 0 & 0 & 0 & 0 & 0 & 0 \\ 0 & 0 & 0 & 0 & \mu\Delta_T & 0 \\ 0 & 0 & 0 & 0 & 0 & \mu\Delta_T \end{pmatrix}, \qquad (9)$$

where $\mathbf{c}_b = \mathbf{s}_b^{-1}$ is the stiffness matrix of the (isotropic) host rock. If both weaknesses (Δ_N and Δ_T) are equal to zero, the medium contains no fractures, while the weaknesses approaching unity correspond to the extreme degree of fracturing. Equation (9) shows that $\Delta_N = 1$ ($c_{11} = 0$) implies the vanishing P-wave velocity in the direction normal to the fractures; likewise, for $\Delta_T = 1$ the S-wave velocity across the fractures goes to zero.

From equation (9) it can be inferred that the stiffnesses of the effective medium are related by $c_{22} = c_{33}$, $c_{12} = c_{13}$, $c_{55} = c_{66}$, and $c_{23} = c_{33} - 2c_{44}$ (note that c_{44} is not influenced by the fractures). Hence, the effective medium is transversely isotropic with a horizontal symmetry axis (HTI medium). Although general HTI models are described by five independent parameters (c_{11}, c_{33}, c_{13}, c_{44}, and c_{55}), the stiffness matrix from equation (9)

depends on just four quantities: λ and μ of the host rock and the dimensionless fracture weaknesses Δ_N and Δ_T. Therefore, there exists a relationship (constraint) between the stiffnesses that can be written as (Schoenberg and Sayers, 1995)

$$c_{11}c_{33} - c_{13}^2 = 2c_{44}(c_{11} + c_{13}). \tag{10}$$

Aligned penny-shaped cracks

One of the simplest models of fractured rock contains a single set of parallel penny-shaped cracks (i.e., the cracks have the form of oblate spheroids) embedded in an isotropic solid. If the semimajor axis of the spheroid is denoted by a and the semiminor axis by c, we can introduce the so-called aspect ratio $\alpha \equiv c/a$, which is much smaller than unity for thin cracks. If the cracks are spheroidal, it is convenient to replace the fracture (crack) intensity by a similar parameter called the crack density, defined as $e = \xi\langle a^3\rangle$, where ξ is the number of cracks per unit volume and $\langle\ \rangle$ denotes volume averaging (Hudson, 1980).

Considering thin, penny-shaped cracks orthogonal to the x_1-axis, Hudson (1980, 1981) derives the following expression for the stiffness matrix $\mathbf{c}$ of the effective medium:

$$\mathbf{c} = \mathbf{c}_b - \frac{e}{\mu}\begin{pmatrix} (\lambda+2\mu)^2U_{11} & \lambda(\lambda+2\mu)U_{11} & \lambda(\lambda+2\mu)U_{11} & 0 & 0 & 0 \\ \lambda(\lambda+2\mu)U_{11} & \lambda^2U_{11} & \lambda^2U_{11} & 0 & 0 & 0 \\ \lambda(\lambda+2\mu)U_{11} & \lambda^2U_{11} & \lambda^2U_{11} & 0 & 0 & 0 \\ 0 & 0 & 0 & 0 & 0 & 0 \\ 0 & 0 & 0 & 0 & \mu^2U_{33} & 0 \\ 0 & 0 & 0 & 0 & 0 & \mu^2U_{33} \end{pmatrix} + O(e^2), \tag{11}$$

where U_{11} and U_{33} are dimensionless quantities that depend on the boundary conditions on the crack faces, infill parameters, possible interaction of cracks, and some other factors. Quadratic and higher order terms in crack density e in equation (11) are ignored. Although the underlying assumptions of Hudson's theory differ from those of the linear slip theory, the effective medium in both cases has the same symmetry (HTI) with the same constraint (10) on the stiffness components.

Comparison of Hudson's and linear-slip models

Schoenberg and Douma (1988) note an even more profound similarity between Hudson's and linear-slip models that goes beyond relationship (10). They point out that matrices (9) and (11) have the same structure and become identical if the fracture weaknesses satisfy the following relations:

$$\Delta_N = \frac{(\lambda+2\mu)}{\mu}U_{11}e, \tag{12}$$

$$\Delta_T = U_{33}e. \tag{13}$$

Equations (12) and (13) can be used to obtain explicit expressions for the weaknesses of dry and fluid-filled cracks. Suppose the fractures are filled with a weak solid with bulk modulus k' and shear modulus μ' (both moduli may be equal to zero). Substituting the expressions for U_{11} and U_{33} given by Hudson (1981) into equations (12) and (13) yields (Schoenberg and Douma, 1988)

$$\Delta_N = \frac{4e}{3g(1-g)\left[1 + \frac{1}{\pi g(1-g)}\left(\frac{k'+4/3\mu'}{\mu}\right)\left(\frac{a}{c}\right)\right]}, \tag{14}$$

$$\Delta_T = \frac{16e}{3(3-2g)\left[1 + \frac{4}{\pi(3-2g)}\left(\frac{\mu'}{\mu}\right)\left(\frac{a}{c}\right)\right]}. \tag{15}$$

The parameter g is defined as

$$g \equiv \frac{\mu}{\lambda+2\mu} = \frac{V_S^2}{V_P^2}, \tag{16}$$

where V_P and V_S are the P- and S-wave velocities in the background medium.

For dry (gas-filled) cracks both moduli of the infill material vanish ($k' = \mu' = 0$), giving

$$\Delta_N = \frac{4e}{3g(1-g)}, \tag{17}$$

$$\Delta_T = \frac{16e}{3(3-2g)}. \tag{18}$$

If the cracks are filled with fluid, the shear modulus is equal to zero ($\mu' = 0$), but the bulk modulus k' for water or oil may be comparable to the shear rigidity μ of the host rock. Hence, for thin cracks with a small aspect ratio c/a, $[(k'+4/3\mu')/\mu](a/c) \gg 1$ and Δ_N goes to zero. However, Δ_T remains the same as for dry cracks. Therefore, for fluid-filled cracks

$$\Delta_N = 0, \tag{19}$$

$$\Delta_T = \frac{16e}{3(3-2g)}. \tag{20}$$

Schoenberg and Sayers (1995) suggest using the ratio K_N/K_T as an indicator of fluid content. They note from existing experiments (Pyrak-Nolte et al., 1990a, b; Hsu and Schoenberg, 1993) that this ratio is close to unity for dry cracks and almost vanishes for fluid-filled ones. To confirm this observation, they infer from Hudson's (1981) theory that for dry cracks

$$K_N/K_T \approx 1 - \sigma/2, \tag{21}$$

where σ is Poisson's ratio for the host rock.

The exact ratio K_N/K_T can be obtained in terms of the weaknesses from equations (7), (8), and (16):

$$\frac{K_N}{K_T} = g\frac{\Delta_N(1-\Delta_T)}{\Delta_T(1-\Delta_N)}. \tag{22}$$

For fluid-filled cracks $K_N/K_T = 0$ because the weakness Δ_N goes to zero.

In the limit of small weaknesses ($\Delta_N \ll 1$ and $\Delta_T \ll 1$), equation (22) reduces to

$$\frac{K_N}{K_T} \approx g\frac{\Delta_N}{\Delta_T}. \tag{23}$$

For dry cracks, we substitute the weaknesses from equations (17) and (18) into equation (23) to find

$$\frac{K_N}{K_T} \approx \frac{3-2g}{4(1-g)} = 1-\sigma/2. \tag{24}$$

Thus, equation (21) is a linearized approximation valid for small fracture weaknesses (i.e., small crack densities). The K_N/K_T ratio from equation (24) varies between 0.75 and 1 for the whole range of g from 0 to 0.5, which seems to confirm the observation of Schoenberg and Sayers (1995).

Calculations based on the exact equation (22), however, may produce K_N/K_T ratios substantially exceeding unity, even if the crack density is small (Figure 1). The discrepancy between the exact and weak-anisotropy results is explained by the influence of the weakness Δ_N in the denominator of equation (22). According to Hudson's (1981) theory, for dry cracks the normal weakness Δ_N is larger than the shear weakness Δ_T and the term $1-\Delta_N$ may be far smaller than unity. It is still unclear whether Hudson's theory, which produces the large values of K_N/K_T for $e = 0.05-0.07$, remains accurate for these crack densities (Ass'ad et al., 1993) because none of the existing experimental measurements (Pyrak-Nolte et al., 1990a,b; Hsu and Schoenberg, 1993) report values of K_N significantly higher than those of K_T.

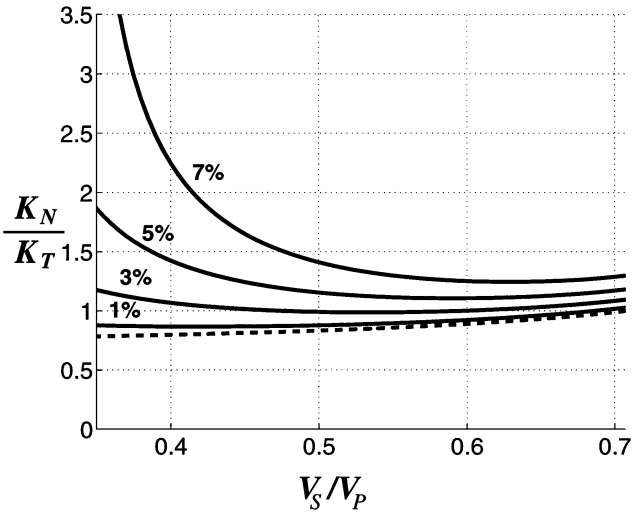

FIG. 1. Ratio of the normal-to-shear fracture compliances in Hudson's model of dry penny-shaped cracks in isotropic host rock. Solid lines—the exact K_N/K_T ratio for different crack densities e (marked on the plot). Dashed line—linearized approximation for K_N/K_T from equation (24).

Thomsen's model of fractured porous media

The weaknesses Δ_N and Δ_T of subsurface fractured rocks may differ substantially from the above estimates obtained for the simplified model of dry or fluid-filled isolated cracks [equations (17)–(20)]. On the one hand, fractures may be stiffened by the cementation of crack (fracture) faces or by the rigidity of the fracture infill. Hudson's theory accounts for these factors by allowing for a nonzero ratio μ'/μ in equations (14) and (15). On the other hand, fluid-filled fractures may be weakened by partial saturation (Hudson, 1988) or fluid flow (squirt) between the fractures and pore space (Thomsen, 1995; Hudson et al., 1996). If the fluid can move under stress from the fractures into hydraulically connected pores, the fractures are no longer stiff enough to preserve the continuity of the normal (orthogonal to their faces) displacement component. Consequently, the weakness Δ_N does not vanish (as it did for isolated cracks completely filled with fluid) and can be expected to take a value intermediate between zero and the Δ_N for gas-filled cracks [see equation (17)]. Thus, the weaknesses Δ_N for fluid- and gas-filled cracks may be considered as the lower and upper bounds (respectively) of this parameter. This conclusion is supported by the work of Thomsen (1995), Hudson (1988), and Hudson et al. (1996).

Thomsen (1995), extending the results of Hoenig (1979), Budiansky and O'Connell (1976), and Hudson (1981), develops a formalism to account for fluid flow between cracks and spherical (isometric) pores. We consider the case of a small concentration of pores [equations (6) and (7) of Thomsen (1995)] so that their equant porosity can be modeled as a dilute distribution of spheres in an isotropic background solid. Then Thomsen's theory also results in an effective stiffness matrix that has the same form as in equation (9). The normal and tangential weaknesses for Thomsen's model are given by

$$\Delta_N = q\Delta_N^{\text{Hudson,dry}} \tag{25}$$

and

$$\Delta_T = \frac{16e}{3(3-2g)}. \tag{26}$$

An explicit expression for the coefficient q can be found in Appendix A. Note that equant porosity has no influence on the tangential weakness, and equation (26) coincides with equation (18) for Δ_T obtained using Hudson's (1981) theory.

Analysis of equations (25), (A-2), and (A-3) shows that in the presence of equant porosity, Δ_N does not vanish, even if the entire pore space is filled with fluid. The parameter q becomes larger with increasing equant porosity, thus making Δ_N closer to that of dry cracks. However, q cannot exceed unity [see equations ((A-1)–(A-3)], which means that Δ_N for Thomsen's model *always* lies between the values for isolated fluid-filled cracks ($\Delta_N = 0$) and dry cracks.

To illustrate the influence of equant porosity on the weaknesses, we computed Δ_N as a function of the V_S/V_P ratio for a wide range of equant porosity values (Figure 2). All curves lie between $\Delta_N = 0$ for isolated fluid-filled cracks [equation (19)] and the dashed line that corresponds to Δ_N for dry cracks [equation (17)]. While Δ_N is almost zero for small equant porosity $\phi_p = 0.01\%$ and $\phi_p = 0.1\%$, it noticeably increases when the porosity $\phi_p = 1\%$ and becomes close to that of dry cracks as ϕ_p reaches 10%.

In summary, all theories examined above lead to the same form of the elastic stiffness tensor that describes a system of parallel, rotationally invariant fractures in a purely isotropic host rock. The effective anisotropic medium is characterized by a special type of the HTI symmetry with four independent stiffness elements. Although each theory operates with a different set of inherent parameters, only four parameter combinations can be extracted from seismic data acquired for such a model. In principle, four measurements of the elastic coefficients may be sufficient to evaluate the Lamé parameters λ and μ of the host rock and two effective fracture parameters—the weaknesses Δ_N and Δ_T. An additional (fifth) measurement is redundant because of constraint (10) and may be used to check the validity of the assumed model.

The most general description of the effective medium is provided by the linear-slip theory, which is directly formulated in terms of the four measurable parameters. Below we discuss how to estimate these parameters from reflection seismic data and use them to evaluate the physical properties of the fracture system.

ANISOTROPIC PARAMETERS OF HTI MEDIA RESULTING FROM VERTICAL FRACTURES

General fracture set

First, let us consider the most general case of a vertical fracture set with the stiffness tensor expressed through the fracture weaknesses in equation (9). Seismic signatures in HTI media are most conveniently described by the vertical velocities (for instance, the P-wave velocity V_{P0} and the velocity $V_{S\perp}$ of the S-wave polarized orthogonal to the cracks) and the following

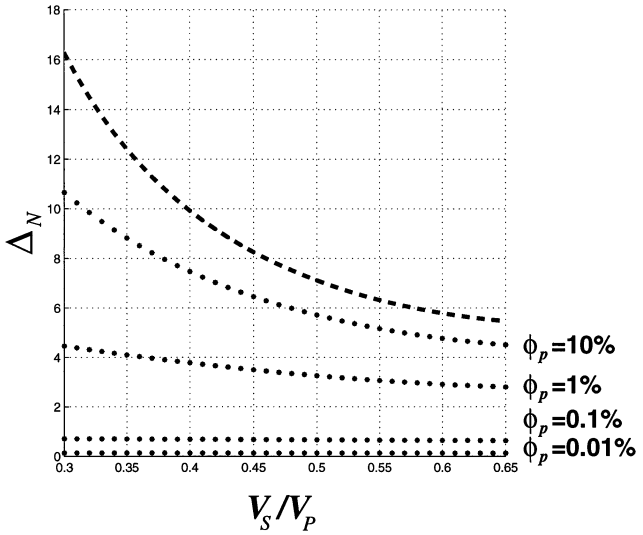

FIG. 2. Influence of equant porosity ϕ_p on the normal weakness of a crack system connected to isometric pores (dotted lines). The dashed line (on top) shows the normal weakness for isolated dry cracks; $\Delta_N = 0$ corresponds to isolated fluid-filled cracks. The vertical scale is in the units of crack density e. The parameters of the crack system are the aspect ratio $\alpha = 0.0005$, the volume portion occupied by the cracks $\phi_c = 0.01\%$, and the crack density $e = 0.05$. The cracks are filled with water that has the bulk modulus $k' = 2$ GPa. The P-wave velocity in the host rock is $V_P = 5$ km/s.

set of anisotropic coefficients introduced by Rüger (1997) and Tsvankin (1997) by analogy with Thomsen's (1986) parameters for VTI media:

$$\epsilon^{(V)} \equiv \frac{c_{11} - c_{33}}{2c_{33}}, \tag{27}$$

$$\delta^{(V)} \equiv \frac{(c_{13} + c_{55})^2 - (c_{33} - c_{55})^2}{2c_{33}(c_{33} - c_{55})}, \tag{28}$$

$$\gamma^{(V)} \equiv \frac{c_{66} - c_{44}}{2c_{44}}. \tag{29}$$

The degree of anellipticity of the model is controlled by the parameter denoted as $\eta^{(V)}$ (Tsvankin, 1997):

$$\eta^{(V)} \equiv \frac{\epsilon^{(V)} - \delta^{(V)}}{1 + 2\delta^{(V)}}. \tag{30}$$

Exact expressions for $\epsilon^{(V)}$, $\delta^{(V)}$, $\gamma^{(V)}$, and $\eta^{(V)}$ in terms of the fracture weaknesses can be derived in a straightforward way from equation (9) and are given in Appendix B. To gain insight into the relationship between the anisotropic coefficients and the fracture weaknesses, equations (B-1)–(B-4) can be linearized with respect to Δ_N and Δ_T under the assumption of weak anisotropy:

$$\epsilon^{(V)} = -2g(1-g)\Delta_N, \tag{31}$$

$$\delta^{(V)} = -2g[(1-2g)\Delta_N + \Delta_T], \tag{32}$$

$$\gamma^{(V)} = -\frac{\Delta_T}{2}, \tag{33}$$

$$\eta^{(V)} = 2g(\Delta_T - g\Delta_N). \tag{34}$$

Analogous expressions for $\epsilon^{(V)}$ and $\delta^{(V)}$ in terms of the fracture compliances K_N and K_T are given by Sayers and Rickett (1997).

Since the squared velocity ratio $g \equiv V_S^2/V_P^2 < 0.5$, we infer from equations (B-1)–(B-4), as well as from equations (31)–(34), that $\epsilon^{(V)}$, $\delta^{(V)}$, and $\gamma^{(V)}$ for vertical fractures are nonpositive:

$$\epsilon^{(V)} \le 0, \quad \delta^{(V)} \le 0, \quad \text{and} \quad \gamma^{(V)} \le 0. \tag{35}$$

An equivalent form of the expression for $\eta^{(V)}$ [derived from equation (B-4)],

$$\eta^{(V)} = (K_T - K_N)\frac{2\mu^2}{\lambda + 2\mu}, \tag{36}$$

shows that the anellipticity parameter is controlled by the difference between the tangential and normal compliances (Schoenberg and Sayers, 1995). Since usually $K_N \le K_T$, $\eta^{(V)}$ is predominantly positive. In the model with gas-filled cracks, however, Hudson's theory predicts that the K_N/K_T ratio may exceed unity with increasing crack density (Figure 1) and $\eta^{(V)}$ may become negative.

As discussed above, the parameters of the crack-induced HTI model satisfy an additional constraint represented through the stiffnesses in equation (10). Rewriting this constraint in terms of the Thomsen-style anisotropic coefficients yields (Tsvankin, 1997)

$$\gamma^{(V)} = -\frac{V_{P0}^2}{2V_{S^\perp}^2}\frac{\epsilon^{(V)}\left[2 - 1/f^{(V)}\right] - \delta^{(V)}}{1 + \sqrt{1 + 2\delta^{(V)}/f^{(V)}} + \left[\epsilon^{(V)} - f^{(V)}\delta^{(V)}\right]/\left[f^{(V)}\left(1 - f^{(V)}\right)\right]}, \tag{37}$$

where V_{P0} is the vertical P-wave velocity, $V_{S^\perp}^2$ is the vertical velocity of the S-wave polarized orthogonal to the cracks, and $f^{(V)} \equiv 1 - V_{S^\perp}^2/V_{P0}^2$. In the linearized weak-anisotropy approximation, equation (37) reduces to

$$\gamma^{(V)} = \frac{1}{4g}\left(\delta^{(V)} - \epsilon^{(V)}\frac{1-2g}{1-g}\right). \tag{38}$$

Approximate relations analogous to equation (38) are given by Schoenberg and Douma (1988) and Thomsen (1995) for TI media formed by parallel horizontal cracks in an isotropic host rock.

As discussed by Tsvankin (1997) and Contreras et al. (1999), equations (37) and (38) suggest that for crack-induced HTI models the shear-wave splitting parameter $|\gamma^{(V)}|$ can be obtained from P-wave moveout data. Indeed, P-wave NMO velocity from horizontal and dipping reflectors can be inverted for the vertical velocity V_{P0}, $\epsilon^{(V)}$, and $\delta^{(V)}$ (Contreras et al., 1999). Then, if an estimate of the V_P/V_S ratio at vertical incidence is available, $\gamma^{(V)}$ can be computed from equation (37).

Possible ranges of anisotropic parameters

The Thomsen-style anisotropic coefficients in the fracture-induced HTI model are controlled by the weaknesses and the ratio of λ and μ, expressed in our notation by $g \equiv V_S^2/V_P^2$. While the shear-wave splitting parameter $\gamma^{(V)}$ is equal to $-\Delta_T/2$ [equation (B-3)], the exact expressions (B-1) and (B-2) for $\epsilon^{(V)}$ and $\delta^{(V)}$ are more complicated. Therefore, it is instructive to study the possible ranges of $\epsilon^{(V)}$ and $\delta^{(V)}$ by varying parameters Δ_N, Δ_T, and g simultaneously within reasonable bounds.

We constrain g by assuming $0.35 \le V_S/V_P \le 0.65$ (or, equivalently, $0.12 \le g \le 0.42$) and use two different ranges for $\gamma^{(V)}$: $|\gamma^{(V)}| \le 0.05$ (equivalently, $\Delta_T \le 0.1$) and $|\gamma^{(V)}| \le 0.15$ (equivalently, $\Delta_T \le 0.3$). For each pair of g and Δ_T within the chosen range, we vary Δ_N from 0 to 1, unless the maximum possible value of the ratio $K_N/K_T = 1$ is reached (we ignore larger values of K_N/K_T produced by Hudson's theory). Figure 3 shows that the possible ranges for both $\epsilon^{(V)}$ and $\delta^{(V)}$ are relatively narrow, especially if $|\gamma^{(V)}| \le 0.05$. The areas of feasible $\epsilon^{(V)}$ and $\delta^{(V)}$ have a quasi-triangular shape and lie above the diagonal that corresponds to the elliptical model, defined by $\epsilon^{(V)} = \delta^{(V)}$ and $\eta^{(V)} = 0$ ($K_N = K_T$).

The values of $\epsilon^{(V)}$ and $\delta^{(V)}$ in Figure 3 were computed using the exact equations (B-1) and (B-2), which are valid for any values of Δ_N and Δ_T between 0 and 1 (hence, for any strength of fracturing). For example, Δ_N in Figure 3b reaches an uncommonly large value of 0.92, which corresponds to extremely compliant fractures that reduce the velocity across them by up to 75% of the background value.

Isolated penny-shaped cracks

Explicit expressions for dry and fluid-filled cracks.—For the special case of thin, isolated, penny-shaped cracks, we can rewrite equations (31)–(34) in terms of the crack density using Hudson 's (1981) theory. To obtain the linearized anisotropic coefficients for dry (or gas-filled) cracks, we substitute equations (17) and (18) for the weaknesses into equations (31)–(34):

$$\epsilon^{(V)} = -\frac{8}{3}e, \tag{39}$$

$$\delta^{(V)} = -\frac{8}{3}e\left[1 + \frac{g(1-2g)}{(3-2g)(1-g)}\right], \tag{40}$$

$$\gamma^{(V)} = -\frac{8e}{3(3-2g)}, \tag{41}$$

$$\eta^{(V)} = \frac{8}{3}e\left[\frac{g(1-2g)}{(3-2g)(1-g)}\right]. \tag{42}$$

Thus, in the weak-anisotropy approximation all parameters become simple functions of the crack density e and the squared V_S/V_P ratio (g) of the host rock. If we assume that the V_S/V_P ratio varies between 0.35 and 0.65, the corresponding ranges of the anisotropic coefficients are

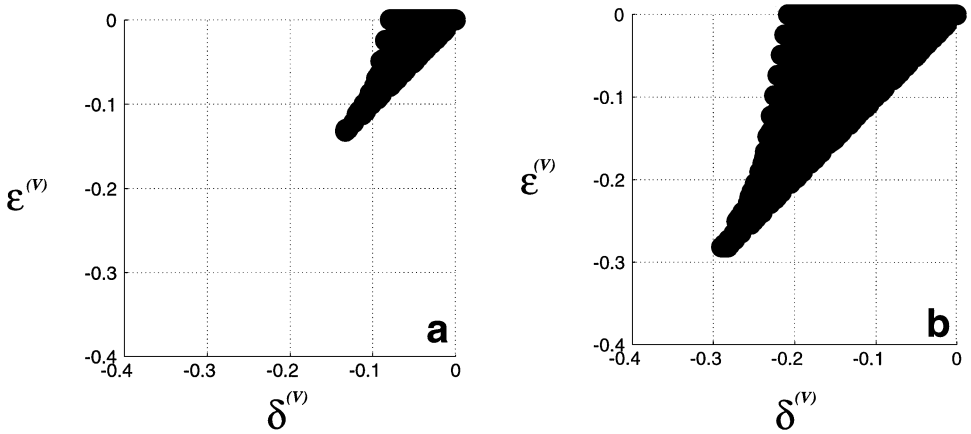

FIG. 3. Possible ranges of the parameters $\epsilon^{(V)}$ and $\delta^{(V)}$ in HTI media resulting from parallel vertical fractures. (a) $|\gamma^{(V)}| \le 0.05$ (or $\Delta_T \le 0.1$); (b) $|\gamma^{(V)}| \le 0.15$ ($\Delta_T \le 0.3$). The V_S/V_P ratio is constrained by $0.12 \le g \le 0.42$, and $K_N/K_T \le 1$.

$$\epsilon^{(V)} = -2.68e,$$
$$\delta^{(V)} = (-2.82 \pm 0.05)e,$$
$$\gamma^{(V)} = (-1.10 \pm 0.13)e,$$
$$\eta^{(V)} = (0.14 \pm 0.05)e. \quad (43)$$

According to equations (43), the HTI medium resulting from dry cracks is close to elliptically anisotropic ($\delta^{(V)} \approx \epsilon^{(V)}$, $\eta^{(V)} \approx 0$), with the parameters largely controlled by the crack density e. Although the only parameter fully independent of g is $\epsilon^{(V)}$, the variations in the other three parameters for the whole range of g are rather insignificant. Note that the shear-wave splitting coefficient $|\gamma^{(V)}|$ is close to e (Thomsen, 1995; Tsvankin, 1997), so the time delay between the split S-waves at vertical incidence gives a good direct estimate of the crack density (a well-known fact often used in fracture characterization).

For fluid-filled cracks, we substitute equations (19) and (20) into equations (31)–(34) to obtain

$$\epsilon^{(V)} = 0, \quad (44)$$
$$\delta^{(V)} = -\frac{32ge}{3(3-2g)}, \quad (45)$$
$$\gamma^{(V)} = -\frac{8e}{3(3-2g)}, \quad (46)$$
$$\eta^{(V)} = -\delta^{(V)} = \frac{32ge}{3(3-2g)}. \quad (47)$$

Fluid saturation does not change the splitting parameter $|\gamma^{(V)}|$ [compare equations (41) and (46)] but has a strong influence on the other anisotropic coefficients. If the cracks are completely saturated with fluid, the P-wave velocities in the directions parallel and orthogonal to the cracks are equal to each other, and $\epsilon^{(V)} = 0$ [equation (44)]. As follows from constraint (38), as well as from equations (45) and (46), for vanishing $\epsilon^{(V)}$

$$\gamma^{(V)} = \frac{\delta^{(V)}}{4g}. \quad (48)$$

For a typical value $g = 0.25$, $\gamma^{(V)}$ and $\delta^{(V)}$ become identical. Therefore, for fluid-filled cracks and $g = 0.25$, the absolute values of $\gamma^{(V)}$, $\delta^{(V)}$, and $\eta^{(V)}$ are close to each other and to the crack density e (Tsvankin, 1997; Rüger and Tsvankin, 1997).

Influence of fluid content.—The influence of fluid saturation on the anisotropic parameters is illustrated in Figure 4. As mentioned above, the presence of fluid has no influence on the shear-wave splitting parameter $\gamma^{(V)}$ because the shear modulus μ' in equation (15) for the weakness Δ_T goes to zero for both dry and fluid-filled cracks.

In contrast, the values of $\epsilon^{(V)}$ for fluid-filled and dry cracks are substantially different; the same conclusion holds for $\delta^{(V)}$. The parameter $\epsilon^{(V)}$ is a function of only one weakness (Δ_N) [equation (31)], which is responsible for the jump of the normal displacement across the crack face and therefore is strongly dependent on the fluid bulk modulus k'. Note that the difference between $\epsilon^{(V)}$ for dry and fluid-filled cracks remains the same ($8e/3$) for any V_S/V_P ratio. For the parameter $\delta^{(V)}$, the influence of the crack infill rapidly decreases with the V_S/V_P ratio. For the most typical $V_S/V_P \approx 0.5$ ($g \approx 0.25$), the absolute value of $\delta^{(V)}$ for dry cracks is almost three times greater than that for fluid-filled cracks.

For models with hydraulically interconnected cracks and pores (Thomsen, 1995) or with partially saturated cracks, the anisotropic parameters always lie between the values for dry and fluid-filled isolated cracks plotted in Figure 4. This follows from the above analysis of equations (25) and (26) and Figure 2.

INVERSION OF SEISMIC SIGNATURES FOR THE PARAMETERS OF HTI MEDIA

Weaknesses Δ_N and Δ_T can be estimated from seismic data if two of the three anisotropic coefficients ($\epsilon^{(V)}$, $\delta^{(V)}$, $\gamma^{(V)}$) and the V_S/V_P ratio are available. For instance, using the linearized weak-anisotropy approximations (31) and (32) for $\epsilon^{(V)}$ and $\delta^{(V)}$, we obtain the weaknesses as

$$\Delta_N = -\frac{\epsilon^{(V)}}{2g(1-g)}, \quad (49)$$
$$\Delta_T = \frac{1}{2g}\left[\frac{1-2g}{1-g}\epsilon^{(V)} - \delta^{(V)}\right]. \quad (50)$$

Equations (49) and (50) indicate that the inversion for Δ_N and Δ_T can be based solely on P-wave traveltime data, which yield $\epsilon^{(V)}$ and $\delta^{(V)}$ (Contreras et al., 1999), assuming that g was estimated independently (e.g., from well logs in the area). Other options include using the azimuthal variation of the P-wave AVO gradient (Rüger, 1997; Rüger and Tsvankin, 1997) or converted (PS) waves; these various approaches are discussed in more detail below.

Further interpretation of the weaknesses in terms of the physical properties of the fracture set is nonunique and cannot be carried out without making assumptions about the

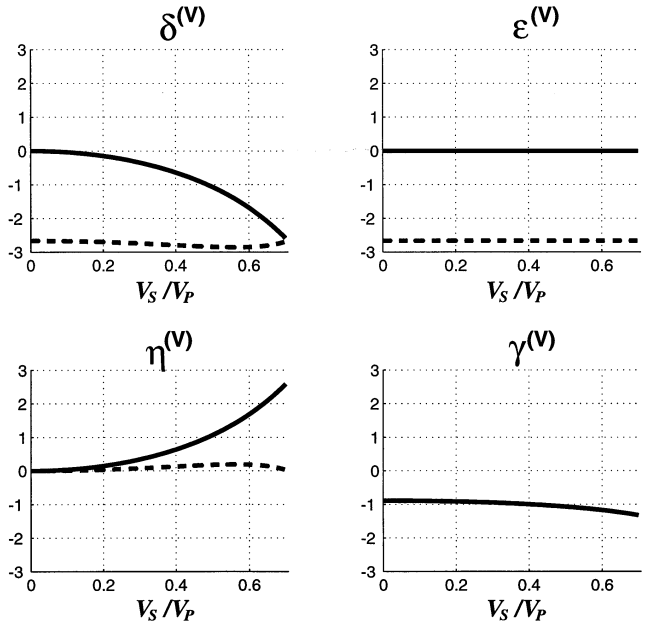

FIG. 4. Anisotropic parameters of the effective HTI model resulting from isolated penny-shaped cracks embedded in an isotropic host rock [from equations (39)–(42) and (44)–(47)]. Solid lines—fluid-filled cracks. Dashed lines—dry (gas-filled) cracks. The vertical scale is in the units of the crack density e.

microstructure of the fractures and pore space. For penny-shaped cracks, possibly connected to isometric pores, the tangential weakness Δ_T depends on only the crack density (i.e., on the strength of fracturing) and remains the same for both dry and fluid-filled cracks [equations (18), (20), and (26)]. The normal weakness Δ_N (and the ratio Δ_N/Δ_T), in contrast, is also a function of fluid content [compare equations (17), (19), and (25)] and thus provides information about fluid saturation in addition to the crack density (see below). Still, for porous formations Δ_N/Δ_T depends not just on fluid saturation but also on the presence of a hydraulic connection between cracks and pore space.

Reflection moveout and AVO gradient of *P*-waves

***P*-wave NMO velocity.—**If the reservoir has a sufficient thickness, information about fracturing can be obtained from the azimuthal variation of the interval NMO velocity. In azimuthally anisotropic media the conventional Dix differentiation, routinely used to recover the interval velocity, becomes inaccurate and must be replaced with a more general expression given by Grechka, Tsvankin, and Cohen (1999). A detailed discussion of the methodology of azimuthal moveout analysis, including a correction for lateral velocity variation, can be found in Grechka and Tsvankin (1999).

Azimuthal variation of P-wave NMO velocity is described by an ellipse in the horizontal plane, even for arbitrary anisotropic heterogeneous media (Grechka and Tsvankin, 1998). In the special case of a plane homogeneous HTI layer, the NMO ellipse is given by (Tsvankin, 1997)

$$V^2_{P,\mathrm{nmo}}(\beta) = V^2_{P0}\frac{1+2\delta^{(\mathrm{V})}}{1+2\delta^{(\mathrm{V})}\sin^2\beta}, \tag{51}$$

where V_{P0} is the P-wave vertical velocity and β is the azimuth of the common-midpoint (CMP) line with respect to the symmetry axis (normal to the fractures). Since $\delta^{(\mathrm{V})} \le 0$, the semimajor axis of the NMO ellipse lies in the fracture plane.

P-wave NMO velocity measurements along three or more well-separated azimuths can be inverted for the fracture orientation, the velocity V_{P0}, and the anisotropic parameter $\delta^{(\mathrm{V})}$. The value of $\epsilon^{(\mathrm{V})}$ (or $\eta^{(\mathrm{V})}$), also required for estimating fracture weaknesses, can be found from NMO velocities of dipping events (Tsvankin, 1997; Contreras et al., 1999) or from nonhyperbolic moveout (Al-Dajani and Tsvankin, 1998).

***P*-wave AVO gradient.—**Reflection coefficients measured at oblique incidence angles over fractured formations vary with the azimuth of the source–receiver line. This azimuthal dependence can be used in AVO analysis to obtain information about the orientation, density, and content of the fractures (Rüger and Tsvankin, 1997; Sayers and Rickett, 1997).

The weak-anisotropy approximation for the plane P-wave reflection coefficient at a small-contrast interface between two HTI media with the same orientation of the symmetry axis is derived by Rüger (1997) in terms of the Thomsen-style anisotropic parameters. The behavior of the reflection coefficient R at small and moderate incidence angles θ is governed by the so-called AVO gradient—the initial slope of R plotted as a function of $\sin^2\theta$. Here we consider the azimuthally varying AVO gradient for a P-wave reflection from the interface between isotropic and HTI media. The difference between the AVO gradients in the directions perpendicular and parallel to the cracks (B^{ani}) can be written as (Rüger, 1997; Rüger and Tsvankin, 1997)

$$B^{\mathrm{ani}} = \frac{\delta^{(\mathrm{V})} - 8g\gamma^{(\mathrm{V})}}{2}, \tag{52}$$

where g has the meaning of the average V_S^2/V_P^2 for the two half-spaces. Substituting the approximate expressions (32) and (33) for $\delta^{(\mathrm{V})}$ and $\gamma^{(\mathrm{V})}$ yields B^{ani} as an explicit function of the fracture weaknesses:

$$B^{\mathrm{ani}} = g[\Delta_T - (1-2g)\Delta_N]. \tag{53}$$

An equivalent equation in terms of the (dimensional) compliances is given by Sayers and Rickett (1997).

For isolated penny-shaped cracks, the azimuthal variation of the AVO gradient can be related directly to the crack density. Equations (40), (41), (45), and (46) for $\delta^{(\mathrm{V})}$ and $\gamma^{(\mathrm{V})}$ obtained from Hudson's (1981) theory lead to the following expressions for dry and fluid-filled fractures:

$$B^{\mathrm{ani}}_{\mathrm{dry}} = \frac{4(-8g^2+12g-3)}{3(3-2g)(1-g)}e, \tag{54}$$

$$B^{\mathrm{ani}}_{\mathrm{wet}} = \frac{16g}{3(3-2g)}e. \tag{55}$$

Clearly, the magnitude of the azimuthal AVO response in weakly anisotropic HTI media is proportional to the crack density. In addition, the value of B^{ani} is strongly dependent on g, i.e., on the V_S/V_P ratio of the host rock (Figure 5). If V_S/V_P takes a typical value of 0.55, $B^{\mathrm{ani}}_{\mathrm{wet}}$ is positive and $B^{\mathrm{ani}}_{\mathrm{dry}}$ is close to

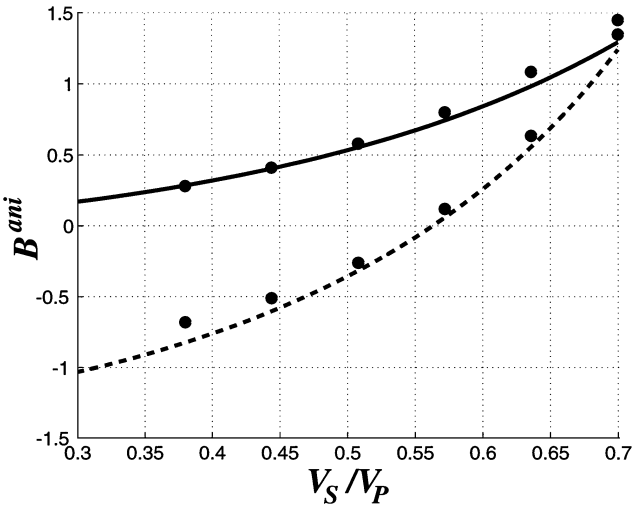

FIG. 5. Azimuthal variation of the AVO gradient for the P-wave reflection from the interface between isotropic and HTI media. The difference between the AVO gradients in the directions perpendicular and parallel to the cracks (B^{ani}) was calculated for dry [equation (54), dashed line] and fluid-filled cracks [equation (55), solid line]. The vertical scale is in the units of the crack density e. The dots mark the values of B^{ani} picked from the curves of the exact reflection coefficient for the crack density $e = 0.07$. The cracks were introduced in the lower half-space using the first-order Hudson's (1981) theory. The upper half-space and the host rock in the lower half-space have the same velocities, with $V_P = 6000$ m/s and V_S changing in accordance with the V_S/V_P ratio on the horizontal axis [$V_S = V_P(V_S/V_P)$]. The densities of the upper and lower media are 2800 and 2300 kg/m^3, respectively.

zero. This result agrees with the computations of Strahilevitz and Gardner (1995), Rüger and Tsvankin (1997), and Sayers and Rickett (1997), who noted that the AVO gradient for dry cracks is almost independent of azimuth for models with similar V_S/V_P ratios. The relation between $B^{\rm ani}_{\rm wet}$ and $B^{\rm ani}_{\rm dry}$, however, changes substantially for higher or lower values of V_S/V_P. For instance, $B^{\rm ani}_{\rm dry} \approx -2\, B^{\rm ani}_{\rm wet}$ when V_S/V_P is close to 0.4. Comparison with the exact reflection coefficient (Figure 5) shows the high accuracy of equations (54) and (55) for moderate crack densities reaching 0.05–0.07.

Thus, the value of $B^{\rm ani}$, combined with an estimate of the V_S/V_P ratio, may serve as an indicator of fluid content. Quantitative interpretation of the azimuthal AVO response, however, requires additional information about the crack density or anisotropic coefficients. Indeed, if the cracks are dry and $V_S/V_P = 0.5 - 0.6$, the P-wave AVO gradient does not vary much with azimuth, irrespective of the degree of fracturing. A direct estimate of the crack density (i.e., Δ_T) can be obtained from shear-wave splitting at vertical incidence; then $B^{\rm ani}$ can be used to find Δ_N [equation (53)] and evaluate fluid saturation. Alternatively, as suggested by Rüger and Tsvankin (1997), the azimuthal AVO response can be combined with the results of azimuthal velocity analysis [equation (51)] to resolve the anisotropic coefficients $\delta^{(\rm V)}$ and $\gamma^{(\rm V)}$, which can be further recalculated into the fracture weaknesses.

As discussed above, if the cracks are partially saturated or are connected to pore space, Δ_N is always greater than zero but is smaller than the value for dry cracks. Equation (53) indicates that $B^{\rm ani}$ in this case falls between the values of $B^{\rm ani}_{\rm wet}$ and $B^{\rm ani}_{\rm dry}$ for the same V_S/V_P ratio. Therefore, the curves shown in Figure 5 define the lower and upper bounds of $B^{\rm ani}$ for various microgeometries of the fractured medium.

Distinguishing between dry and fluid-filled cracks.—Let us assume that two anisotropic parameters [for example, $\epsilon^{(\rm V)}$ and $\delta^{(\rm V)}$] have been found and an estimate of g is available. Then it is important to assess whether one can distinguish between dry and fluid-filled cracks in the presence of realistic errors in $\epsilon^{(\rm V)}$, $\delta^{(\rm V)}$, and V_S/V_P ratio (g).

First, consider a fracture set with the density $e = 7\%$ embedded in a medium with $V_S/V_P = 0.5$ ($g = 0.25$). For such a model, the tangential weakness $\Delta_T = 0.15$ for both dry and fluid-filled cracks, while the normal weakness changes from $\Delta_N = 0.50$ if the cracks are dry ($\epsilon^{(\rm V)} = -0.21$, $\delta^{(\rm V)} = -0.19$) to $\Delta_N = 0$ for fluid-filled cracks ($\epsilon^{(\rm V)} = 0$, $\delta^{(\rm V)} = -0.07$). We simulated errors in the data by adding Gaussian noise with the standard deviation $\sigma = 0.05$ to the correct values of $\epsilon^{(\rm V)}$, $\delta^{(\rm V)}$, and V_S/V_P and inverted these three parameters for Δ_N and Δ_T using the exact equations from Appendix B. The inversion results, along with the input anisotropic coefficients, are marked by small dots in Figure 6. Clearly, the clouds of estimated weaknesses are well separated by their values of Δ_N. This implies that although errors in $\epsilon^{(\rm V)}$, $\delta^{(\rm V)}$, and V_S/V_P on the order of $\pm 0.05 - 0.1$ introduce a substantial uncertainty in the value of the crack density (or Δ_T), they do not prevent us from separating models with dry and fluid-filled cracks.

Figure 7 displays the results of some additional numerical experiments. As expected, reducing errors in the data leads to a visible tightening of the clouds of Δ_N and Δ_T (compare Figures 7a and 7b with Figures 6c and 6d). With decreasing data error, it may become possible to distinguish between fully and partially saturated fractures (or fractures connected to pore space).

The sensitivity of the weaknesses to errors in input data (reflected in the size of the Δ_N and Δ_T clouds) is controlled by the V_S/V_P ratio (Figures 7c–f). For a fixed magnitude of errors in $\epsilon^{(\rm V)}$ and $\delta^{(\rm V)}$, the errors in Δ_N and Δ_T decrease with increasing V_S/V_P ratio. However, the value of Δ_N for dry cracks also decreases from $\Delta_N = 0.7$ for $V_S/V_P = 0.4$ to $\Delta_N = 0.4$ for $V_S/V_P = 0.6$ (Figures 7d and 7f). As a result, the separation between Δ_N for the models with dry and fluid-filled cracks is smaller for higher V_S/V_P ratios, and our overall ability to resolve the fluid content is almost independent of the V_S/V_P ratio.

Our numerical tests thus suggest that it is feasible to distinguish between dry and fluid-filled fractures if errors in $\epsilon^{(\rm V)}$, $\delta^{(\rm V)}$, and the V_S/V_P ratio do not exceed 0.1 and the crack density reaches 5–7%.

Reflection moveout and AVO gradient of *PS*-waves

For multicomponent surveys, it is possible to devise a fracture-detection algorithm based on mode-converted (PS) data. Since moveout and amplitude information average medium properties on different scales, combining the P-wave NMO velocity and AVO gradient in the characterization of heterogeneous formations may prove difficult. Therefore, it is advantageous to supplement the P-wave NMO ellipse with reflection traveltimes of PS-waves or, alternatively to carry out joint inversion of the AVO gradients of P- and PS-waves.

One of the split shear waves in HTI media (denoted as $S^{\parallel}$ or S parallel) is polarized in the isotropy (fracture) plane, while the polarization vector of the second S-wave ($S^{\perp}$) lies in the plane

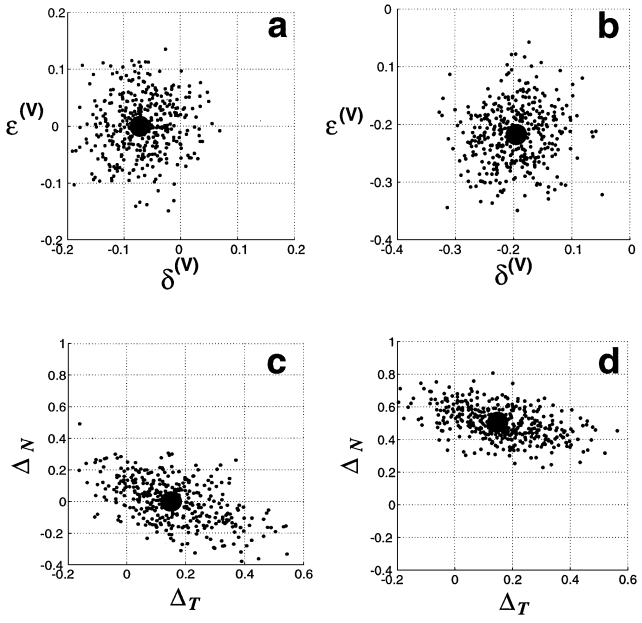

FIG. 6. Noise-contaminated anisotropic coefficients $\epsilon^{(\rm V)}$ and $\delta^{(\rm V)}$ for (a) fluid-filled and (b) dry cracks (small dots). (c) The inverted weaknesses Δ_N and Δ_T for the fluid-filled model from (a). (d) The inverted Δ_N and Δ_T for the dry-crack model from (b). The large dots indicate the correct parameter values.

formed by the symmetry axis and the slowness vector. At vertical incidence, the $S^{\perp}$-wave is polarized perpendicular to the fractures and travels slower than the $S^{\parallel}$-wave. In each vertical symmetry plane, the P-wave is coupled to the in-plane polarized S-wave and generates a single converted-mode reflection from a horizontal interface. Thus, in the isotropy (fracture) plane one should be able to record the reflected wave $PS^{\parallel}$, while in the plane orthogonal to the fractures (the symmetry-axis plane) an incident P-wave is converted into the $PS^{\perp}$ reflection. Since either one or the other of the two converted modes is weak in the vicinity of each symmetry plane, extracting the full azimuthal dependence of the NMO velocity or AVO gradient of the $PS^{\parallel}$- or $PS^{\perp}$-wave requires a better azimuthal coverage than that for P-wave reflections. Here, we restrict the discussion to the reflection traveltimes and amplitudes of converted waves in the vertical symmetry planes of the HTI medium.

***PS*-wave traveltimes.**—As follows from the analysis of Grechka, Theophanis, and Tsvankin (1999) for the more general orthorhombic media, the azimuthal variation of the NMO velocity of each converted wave ($PS^{\parallel}$ and $PS^{\perp}$) in a horizontal HTI layer is elliptical. By performing moveout (semblance) analysis in the symmetry planes, we determine the vertical traveltime and one of the semiaxes of the NMO ellipse for each converted wave. Note that mode conversions in a horizontal HTI layer vanish at vertical incidence, and the vertical (zero-offset) traveltimes of the converted waves are found essentially by extrapolation using the best-fit hyperbola provided by semblance analysis.

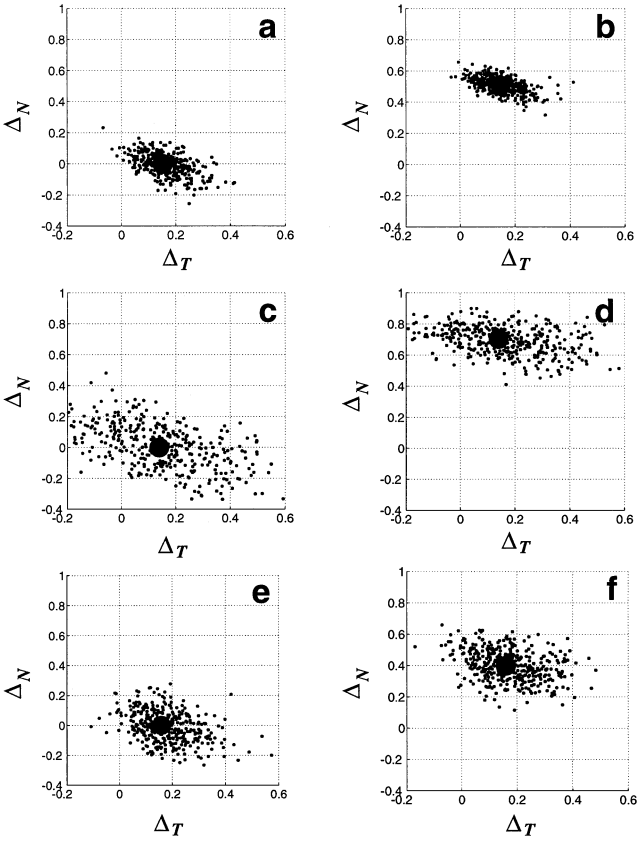

FIG. 7. Dependence of the inverted weaknesses Δ_N and Δ_T (small dots) for fluid-filled (left column) and dry (right column) cracks on the V_S/V_P ratio and on the standard deviation σ of $\epsilon^{(V)}$, $\delta^{(V)}$, and V_S/V_P from their correct values. The weaknesses are the same as in Figure 6. (a) and (b): $\sigma = 0.025$, $V_S/V_P = 0.5$. (c) and (d): $\sigma = 0.05$, $V_S/V_P = 0.4$. (e) and (f): $\sigma = 0.05$, $V_S/V_P = 0.6$.

Given the P-wave zero-offset reflection traveltime, the zero-offset times of the converted waves from the same interface can be used to obtain the ratio of the shear-wave vertical velocities [i.e., the parameter $\gamma^{(V)}$] and an estimate of the ratio $g \equiv V_S^2/V_P^2$. This implies that the P-wave NMO ellipse, which provides $\delta^{(V)}$, and the vertical traveltimes of the P-wave and split converted waves are sufficient to find $\gamma^{(V)}$, $\delta^{(V)}$, and g and, therefore, both fracture weaknesses.

Symmetry-plane NMO velocities of the converted waves provide redundant information that may, however, increase the accuracy of the parameter estimation procedure. In each vertical symmetry plane the traveltimes of reflected waves are described by the same equations as in VTI media, and the NMO velocities of P-, S-, and PS-waves are related by the following Dix-type equation (Tsvankin and Thomsen, 1994):

$$[V_{S,\mathrm{nmo}}]^2 = \frac{t_0^{(PS)}[V_{PS,\mathrm{nmo}}]^2 - t_0^{(P)}[V_{P,\mathrm{nmo}}]^2}{t_0^{(PS)} - t_0^{(P)}}, \qquad (56)$$

where t_0 denotes the one-way vertical traveltime for pure (P and S) reflections and the two-way vertical traveltime for the PS-wave. Equation (56) can be used to obtain the NMO velocities of the reflected shear waves $S^{\parallel}$ (in the fracture plane) and $S^{\perp}$ (in the plane perpendicular to the fractures) from P and PS data. Since the velocity of each mode in the fracture plane is independent of the angle with the vertical, the NMO velocity of the $S^{\parallel}$-wave is equal to the fast shear-wave vertical velocity V_{S1}. The NMO velocity of the $S^{\perp}$-wave in the direction perpendicular to the fractures is given by (Tsvankin, 1997)

$$V_{S^{\perp},\mathrm{nmo}} = V_{S2}\sqrt{1 + 2\sigma^{(V)}} \qquad (57)$$

and

$$\sigma^{(V)} \equiv \left(\frac{V_{P0}}{V_{S2}}\right)^2 \left(\epsilon^{(V)} - \delta^{(V)}\right), \qquad (58)$$

where V_{P0} and V_{S2} are the vertical velocities of the P- and $S^{\perp}$-waves, respectively. If the vertical velocities and $\delta^{(V)}$ were determined from the P-wave NMO ellipse and the vertical traveltimes, the NMO velocity of the $S^{\perp}$-wave yields $\epsilon^{(V)}$. Both the fast S-wave velocity V_{S1} and $\epsilon^{(V)}$, however, can be obtained as well from the vertical traveltimes of the converted waves, the P-wave NMO ellipse, and the constraint on the anisotropic parameters of HTI media.

***PS*-wave AVO gradient.**—For relatively thin target layers, interval moveout analysis becomes inaccurate; so it may be advantageous to supplement the P-wave AVO response with prestack amplitudes of PS-wave reflections. Of course, it is also possible to use nonconverted shear waves, but they are seldom acquired in exploration surveys.

As before, we consider an interface between isotropic and HTI media and analyze the magnitude of the azimuthal variation of the reflection coefficient. The results of Rüger (1996) show that the PS reflection coefficient at small offsets is proportional to $\sin\theta$, where θ is the P-wave incidence angle.

Therefore, we define the PS-wave AVO gradient as the coefficient of the $\sin\theta$ term and use Rüger's (1996) weak-anisotropy approximations to express the AVO gradient through the anisotropic parameters. The difference between the AVO gradients of the $PS^{\perp}$-wave across the fractures and the $PS^{\parallel}$-wave parallel to them can be written as

$$B^{\text{ani}} = \frac{\delta_2^{(V)} - 4(\sqrt{g} + g)\gamma_2^{(V)}}{2(1 + \sqrt{g})}. \qquad (59)$$

Introducing the fracture weaknesses into equation (59) yields

$$B^{\text{ani}} = \frac{\sqrt{g}}{1 + \sqrt{g}}[\Delta_T - \sqrt{g}(1 - 2g)\Delta_N]. \qquad (60)$$

Despite some similarity between equation (60) and the corresponding P-wave expression (53), the factor B^{ani} for the P- and PS-modes is controlled by different combinations of Δ_T and Δ_N. Hence, using both P- and PS-waves in azimuthal AVO analysis has the potential of yielding information on the weaknesses Δ_T and Δ_N or, equivalently, the crack density and the fluid content of the fractures. Also, as mentioned, the squared vertical-velocity ratio g may be determined from the P- and PS-wave traveltimes, unless the reservoir is too thin.

Figure 8 reproduces the numerical example from Figure 5 but this time for PS-waves. The curves were generated by substituting the values of Δ_N and Δ_T for dry (dashed line) and fluid-filled (solid) cracks into equation (60). Note that the accuracy of the weak-anisotropy approximation for the PS-wave is not much lower than that for the P-wave. As expected from the form of the analytic solutions, B^{ani} for both P- and PS-waves is positive in models with isolated fluid-filled cracks and changes sign with increasing V_S/V_P for dry cracks. However, in the latter case the intersection with the horizontal axis for PS-waves occurs at a lower value of V_S/V_P than for P-waves. Hence, if the V_S/V_P ratio is close to a typical value of 0.55 and the P-wave AVO gradient for dry cracks is almost independent of azimuth

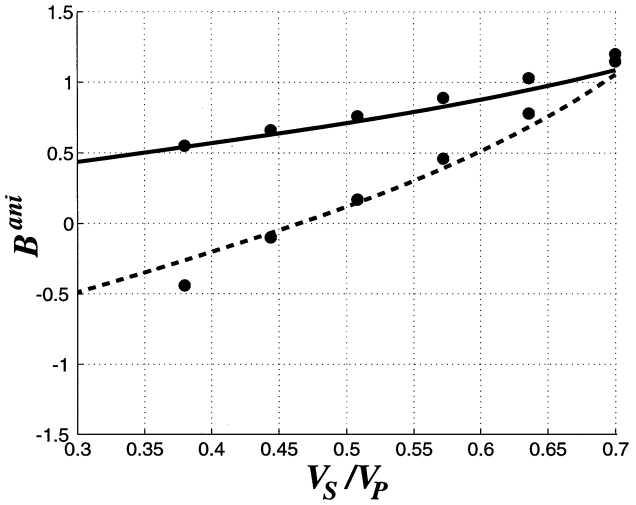

FIG. 8. The difference between the converted-wave AVO gradients in the directions perpendicular ($PS^{\perp}$) and parallel ($PS^{\parallel}$) to the cracks for dry (dashed line) and fluid-filled (solid line) cracks; both curves are computed from the weak-anisotropy approximation. The dots mark the values of B^{ani} picked from the curves of the exact reflection coefficient for the crack density $e = 0.07$. The model parameters are the same as those in Figure 5.

(Rüger and Tsvankin, 1997; Sayers and Rickett, 1997), the addition of PS-waves may help identify fracturing and, moreover, discriminate between dry and fluid-filled cracks.

DISCUSSION AND CONCLUSIONS

The linear-slip theory (e.g., Schoenberg and Sayers, 1995), based on the general treatment of fractures as surfaces of weakness inside a solid matrix, provides a convenient framework for relating seismic signatures to the properties of fracture systems. The inherent parameters of the linear–slip theory for rotationally invariant fractures are the normal (Δ_N) and tangential (Δ_T) weaknesses, which can be estimated from seismic data. The theories of Hudson (1981) and Thomsen (1995), designed for specific physical fracture models involving penny-shaped cracks, can be used to express Δ_N and Δ_T through parameters dependent on the microstructure of cracks and pores. Although determination of these microstructural parameters from seismic data requires additional information about the medium, Hudson's and Thomsen's models are helpful in guiding the interpretation of the weaknesses in terms of the crack density and fluid content.

Vertical, parallel, rotationally invariant fractures lead to a particular type of HTI media described by four independent parameters. We obtained linearized expressions for the Thomsen-style anisotropic coefficients of HTI media $\epsilon^{(V)}$, $\delta^{(V)}$, and $\gamma^{(V)}$ in terms of the weaknesses Δ_N and Δ_T and the V_S/V_P ratio in the background medium. One of the anisotropic parameters ($\epsilon^{(V)}$, $\delta^{(V)}$, or $\gamma^{(V)}$) can be found from the other two and the V_S/V_P ratio. Interestingly, $\epsilon^{(V)}$, $\delta^{(V)}$, and $\gamma^{(V)}$ in any fracture-induced HTI model are always negative, while the anellipticity parameter $\eta^{(V)}$ is predominantly positive. All possible pairs $[\epsilon^{(V)}, \delta^{(V)}]$ for HTI models resulting from parallel vertical fractures belong to a relatively narrow area with a quasi-triangular shape on the $[\epsilon^{(V)}, \delta^{(V)}]$-plane. These results can be used to identify fracture-induced HTI media from seismic measurements.

If the model contains isolated penny-shaped (spheroidal) cracks, the weaknesses and the anisotropic parameters can be related to the physical properties of the crack system using Hudson's theory. In the linearized weak-anisotropy approximation, all anisotropic parameters are proportional to the crack density, with the coefficients controlled by the V_S/V_P ratio and, for $\epsilon^{(V)}$ and $\delta^{(V)}$, fluid saturation. The shear-wave splitting parameter $|\gamma^{(V)}|$ for dry or fluid-filled cracks and a wide range of the V_S/V_P ratios remains close to the crack density. Therefore, the traveltimes or reflection amplitudes of split S-waves at vertical incidence are strongly dependent on the degree of fracturing but cannot be used to discriminate between dry and fluid-filled cracks.

In contrast, $\epsilon^{(V)}$ and $\delta^{(V)}$ are sensitive to the presence of fluid in the cracks. If the cracks are dry, the effective medium is close to elliptical ($\epsilon^{(V)} \approx \delta^{(V)}$), with the anisotropic parameters tightly governed by the crack density and weakly dependent on the V_S/V_P ratio. The absolute value of $\epsilon^{(V)} \approx \delta^{(V)}$ for dry cracks is almost three times higher than $|\gamma^{(V)}|$ and the crack density. For isolated fluid-filled cracks, $\epsilon^{(V)}$ practically vanishes, while $\delta^{(V)}$ for typical $V_S/V_P \approx 0.5$ is close to $\gamma^{(V)}$ and (by absolute value) to the crack density. The influence of crack infill on $\delta^{(V)}$, however, decreases with the V_S/V_P ratio. For models with interconnected cracks and pores (Thomsen, 1995) or with

partially saturated cracks, $\epsilon^{(V)}$ and $\delta^{(V)}$ always lie between the values for dry and isolated fluid-filled cracks.

The simplest way to estimate $\delta^{(V)}$ and the fracture orientation is to reconstruct the P-wave NMO ellipse from a horizontal reflector by means of azimuthal moveout analysis. The parameter $\epsilon^{(V)}$ can also be obtained from P-wave data using dipping events or nonhyperbolic moveout. Then $\epsilon^{(V)}$ and $\delta^{(V)}$, along with the V_S/V_P ratio, which must be evaluated separately (e.g., from well logs in the area), can be used to find $\gamma^{(V)}$. Alternatively, $\gamma^{(V)}$ can be determined directly from prestack P-wave amplitudes by combining the azimuthal variation of the AVO gradient with the NMO ellipse for horizontal events. If converted waves are available and the reservoir is sufficiently thick, it is possible to recover all relevant anisotropic parameters from the zero-offset traveltimes of P- and PS-waves and either the P-wave NMO ellipse or the AVO gradients of the P- or PS-waves. For surveys acquired with shear-wave sources, it is beneficial to calibrate P-wave data with split shear waves, whose polarizations, traveltimes, and AVO response give an independent estimate of the fracture orientation and parameter $\gamma^{(V)}$ and help to evaluate the V_S/V_P ratio.

Any two out of the three anisotropic parameters ($\epsilon^{(V)}$, $\delta^{(V)}$, and $\gamma^{(V)}$) and the V_S/V_P ratio can then be recalculated into the fracture weaknesses Δ_N and Δ_T. Further interpretation of the weaknesses is not unique and must rely on the assumed physical model. For penny-shaped cracks, the tangential weakness is close to twice the crack density, while the normal weakness, Δ_N, (or the ratio Δ_N/Δ_T) is sensitive to fluid saturation. Even for moderate crack densities, there is a substantial difference between the value of Δ_N for dry cracks and the vanishing Δ_N for isolated fluid-filled cracks, with intermediate values of the normal weakness corresponding to partial saturation and/or the presence of fluid flow (squirt) between cracks and pore space. Therefore, Δ_N/Δ_T is a useful indicator of fluid content, although its interpretation may be ambiguous without additional information.

ACKNOWLEDGMENTS

This research was carried out during a visit of Andrey Bakulin to the Center for Wave Phenomena (CWP), Colorado School of Mines, in 1998. We are grateful to Leon Thomsen (BP Amoco) and members of the A (nisotropy)-team of CWP for helpful discussions and to Andreas Rüger (Landmark) for his review of the manuscript. The support for this work was provided by the members of the Consortium Project on Seismic Inverse Methods for Complex Structures at CWP and by the U.S. Department of Energy (award #DE-FG03-98ER14908).

REFERENCES

Aguilera, R., 1998, Geologic aspects of naturally fractured reservoirs: The Leading Edge, **17**, 1667–1670.
Al-Dajani, A., and Tsvankin, I., 1998, Nonhyperbolic reflection moveout for horizontal transverse isotropy: Geophysics, **63**, 1738–1753.
Ass'ad, J. M., Tatham, R. H., McDonald, J. A., Kusky, T. M., and Jech, J., 1993, A physical model study of scattering of waves by aligned cracks: Comparison between experiment and theory: Geophys. Prosp., **41**, 323–339.
Backus, G. E., 1962, Long-wave elastic anisotropy produced by horizontal layering: J. Geophys. Res., **67**, 4427–4440.
Bagrintseva, K. I., 1982, Fracturing of rocks: Nedra (in Russian).
Bakulin, A. V., and Molotkov, L. A., 1998, Effective models of fractured and porous media: St. Petersburg Univ. Press (in Russian).
Berg, E., Hood, J., and Fryer, G., 1991, Reduction of the general fracture compliance matrix Z to only five independent elements: Geophys. J. Internat., **107**, 703–707.
Budiansky, B., and O'Connell, R. J., 1976, Elastic moduli of a cracked solid: Internat. J. Solids Structures, **12**, 81–97.
Contreras, P., Grechka, V., and Tsvankin, I., 1999, Moveout inversion of P-wave data for horizontal transverse isotropy: Geophysics, **64**, 1219–1229.
Corrigan, D., Withers, R., Darnall, J., and Skopinski, T., 1996, Fracture mapping from azimuthal velocity analysis using 3D surface seismic data: 66th Ann. Internat. Mtg., Soc. Expl. Geophys., Expanded Abstracts, 1834–1837.
Grechka, V., and Tsvankin, I., 1998, 3-D description of normal moveout in anisotropic inhomogeneous media: Geophysics, **63**, 1079–1092.
———1999, 3-D moveout inversion in azimuthally anisotropic media with lateral velocity variation: Theory and a case study: Geophysics, **64**, 1202–1218.
Grechka, V., Theophanis, S., and Tsvankin, I., 1999, Joint inversion of P- and PS-waves in orthorhombic media: Theory and a physical-modeling study: Geophysics, **64**, 146–161.
Grechka, V., Tsvankin, I., and Cohen, J. K., 1999, Generalized Dix equation and analytic treatment of normal-moveout velocity for anisotropic media: Geophys. Prosp., **47**, 117–148.
Hoenig, A., 1979, Elastic moduli of the non-randomly cracked body: Internat. J. Solids Structures, **15**, 137–154.
Hsu, C.-J., and Schoenberg, M., 1993, Elastic waves through a simulated fractured medium: Geophysics, **58**, 964–977.
Hudson, J. A., 1980, Overall properties of a cracked solid: Math. Proc. Camb. Phil. Soc., **88**, 371–384.
———1981, Wave speeds and attenuation of elastic waves in material containing cracks: Geophys. J. Roy. Astr. Soc., **64**, 133–150.
———1988, Seismic wave propagation through material containing partially saturated cracks: Geophys. J., **92**, 33–37.
Hudson, J. A., Liu, E., and Crampin, S., 1996, The mechanical properties of materials with interconnected cracks and pores: Geophys. J. Internat., **124**, 105–112.
Kirkinskaya, V. N., and Smekhov, E. M., 1981, Carbonate rocks as collectors of oil and gas: Nedra (in Russian).
Molotkov, L. A., and Bakulin, A. V., 1997, An effective model of a fractured medium with fractures modeled by the surfaces of discontinuity of displacements: J. Math. Sci., **86**, 2735–2746.
Nichols, D., Muir, F., and Schoenberg, M., 1989, Elastic properties of rocks with multiple sets of fractures: 59th Ann. Internat. Mtg., Soc. Expl. Geophys., Expanded Abstracts, 471–474.
Pyrak-Nolte, L. J., Myer, L. R., and Cook, N. G. W., 1990a, Transmission of seismic waves across single natural fractures: J. Geophys. Res., **95**, No. B6, 8617–8638.
———1990b, Anisotropy in seismic velocities and amplitudes from multiple parallel fractures: J. Geophys. Res., **95**, No. B7, 11 345–11 358.
Romm, E. S., 1985, Structural models of rocks pore space: Nedra (in Russian).
Rüger, A., 1996, Reflection coefficients and azimuthal AVO analysis in anisotropic media: Ph.D. thesis, Colorado School of Mines.
———1997, P-wave reflection coefficients for transversely isotropic models with vertical and horizontal axis of symmetry: Geophysics, **62**, 713–722.
Rüger, A., and Tsvankin, I., 1997, Using AVO for fracture detection: Analytic basis and practical solutions: The Leading Edge, **10**, 1429–1434.
Sayers, C., and Rickett, J. E., 1997, Azimuthal variation in AVO response for fractured gas sands: Geophys. Prosp., **45**, 165–182.
Schoenberg, M., 1980, Elastic wave behavior across linear slip interfaces: J. Acoust. Soc. Am., **68**, 1516–1521.
——1983, Reflection of elastic waves from periodically stratified media with interfacial slip: Geophys. Prosp., **31**, 265–292.
Schoenberg, M., and Douma, J., 1988, Elastic wave propagation in media with parallel fractures and aligned cracks: Geophys. Prosp., **36**, 571–590.
Schoenberg, M., and Muir, F., 1989, A calculus for finely layered anisotropic media: Geophysics, **54**, 581–589.
Schoenberg, M., and Sayers, C., 1995, Seismic anisotropy of fractured rock: Geophysics, **60**, 204–211.
Strahilevitz, R., and Gardner, G. H. F., 1995, Fracture detection using P-wave AVO: 65th Ann. Internat. Mtg., Soc. Expl. Geophys., Expanded Abstracts, 589–591.
Thomsen, L., 1986, Weak elastic anisotropy: Geophysics, **51**, 1954–1966.
———1995, Elastic anisotropy due to aligned cracks in porous rock: Geophys. Prosp., **43**, 805–830.
Tsvankin, I., 1997, Reflection moveout and parameter estimation for horizontal transverse isotropy: Geophysics, **62**, 614–629.
Tsvankin, I., and Thomsen, L., 1994, Nonhyperbolic reflection moveout in anisotropic media: Geophysics, **59**, 1290–1304.

APPENDIX A

WEAKNESSES FOR THOMSEN'S MODEL OF FRACTURED POROUS ROCK

Thomsen (1995) has developed a model that accounts for the effect of fluid flow (squirt) between cracks and isometric pores in porous rocks. He generalizes the results of Hoenig (1979), Budiansky and O'Connell (1976), and Hudson (1981) for the model that contains two sets of hydraulically connected inclusions (e.g, the first set is thin cracks and the second is isometric pores). Here we restrict the discussion to models with a small concentration of isometric pores [equations (6) and (7) of Thomsen (1995)], where equant porosity is approximated by a dilute distribution of spherical pores in an isotropic matrix.

The expressions for the generic Thomsen parameters ϵ, δ, and γ for this medium (Thomsen, 1995) become identical to those for the linear-slip model (Schoenberg and Douma, 1988), if we use the following expressions for Δ_N and Δ_T:

$$\Delta_N = \frac{4}{3}\frac{e}{(1-g)g}\left(1-\frac{k'}{\lambda+2/3\mu}\right)D_{\rm cp}, \qquad \Delta_T = \frac{16}{3}\frac{e}{(3-2g)}. \tag{A-1}$$

Here λ and μ are the Lamé parameters of the matrix, k' is the bulk modulus of the fluid filling the cracks ($\mu'=0$), e is the crack density, $g \equiv V_S^2/V_P^2$, and $D_{\rm cp}$ is the so-called fluid factor, designed to account for the interconnection between cracks and pores. At relatively low frequencies, where the fluid has enough time to move from cracks to pores, $D_{\rm cp}$ is given by (Thomsen, 1995)

$$D_{\rm cp} = \left[1-\frac{k'}{\lambda+2/3\mu}+\frac{k'}{(\lambda+2/3\mu)(\phi_c+\phi_p)}\times(A_p\phi_p+A_c e)\right]^{-1}, \tag{A-2}$$

where ϕ_p and ϕ_c are the fractions of volume occupied by pores and cracks, respectively [the crack porosity may be expressed as $\phi_c=(4\pi ec)/(3a)$]. Coefficients A_p and A_c depend only on the background V_S/V_P ratio: $A_p=(3-2g)/(2g)$ and $A_c=(4/9)\times[(2-3g)/(1-g)]$ (Thomsen, 1995). Comparing equation (A-1) with (17), we may represent the normal weakness for the Thomsen model as

$$\Delta_N = q\,\Delta_N^{\rm Hudson,\,dry}, \quad q=\left(1-\frac{k'}{\lambda+2/3\mu}\right)D_{\rm cp}. \tag{A-3}$$

APPENDIX B

EXACT EXPRESSIONS FOR THE ANISOTROPIC COEFFICIENTS OF TERMS OF THE WEAKNESSES

The exact expressions for the anisotropic coefficients $\epsilon^{(V)}$, $\delta^{(V)}$, and $\gamma^{(V)}$ in terms of the weaknesses Δ_N and Δ_T can be derived from equations (9) and (27)–(29) as

$$\epsilon^{(V)} = -\frac{2g(1-g)\Delta_N}{1-\Delta_N(1-2g)^2}, \tag{B-1}$$

$$\delta^{(V)} = -\frac{2g[(1-2g)\Delta_N+\Delta_T][1-(1-2g)\Delta_N]}{\left[1-\Delta_N(1-2g)^2\right]\left[1+\frac{1}{1-g}\left(\Delta_T-\Delta_N(1-2g)^2\right)\right]}, \tag{B-2}$$

and

$$\gamma^{(V)} = -\frac{\Delta_T}{2}. \tag{B-3}$$

The exact anellipticity coefficient $\eta^{(V)}$ is proportional to the difference between the shear and normal compliances:

$$\eta^{(V)} = (K_T-K_N)\times\frac{2\mu^2(\lambda+\mu)(1+K_N(\lambda+2\mu))}{(\lambda+\mu)(\lambda+2\mu)(1+2K_N\mu)^2+\lambda^2\mu(K_T-K_N)}. \tag{B-4}$$

Schoenberg and Sayers (1995) were the first to point out that the sign of anellipticity is controlled by the difference K_T-K_N.